*Electronic Supplementary Information*

# Multifunctional Gradient Hydrogel with Ultrafast Thermo-Responsive Actuation and Ultrahigh Conductivity

He Liu[a], Xueying Jia[b], Ruonan Liu[a], Kun Chen[a], Zhaoyang Wang[a], Tong Lyu[a], Xiaoyu Cui[a], Yue Zhao[a] and Ye Tian[a, c*]

[a] College of Medicine and Biological Information Engineering, Northeastern University, Shenyang 110169, China

[b] School of International Education, Northeastern University, Shenyang 110169, China

[c] Foshan Graduate School of Northeastern University, Foshan, 528300, China

E-mail: tianye@bmie.neu.edu.cn

**Contents**

**Supplementary Notes, Tables, Figures and Movies**

**Supplementary Note 1.** Wettability-based strategy.

**Supplementary Note 2.** Octopus-tentacle inspired hydrogel.

**Table S1.** Summarization for the bending speed and bending amplitude of hydrogel actuators.

**Table S2.** Comparison of the main conductive parameters of Ag-PNIPAM hydrogel and conductive hydrogel strain sensors in previous mainstream work.

**Table S3.** Summarization for the gripping time and the releasing time of hydrogel gripper.

**Fig. S1.** The water contact angles of Ag-PNIPAM hydrogel.

**Fig. S2.** Distribution of Ag content in Ag-PNIPAM hydrogel.

**Fig. S3.** FTIR spectra of pure PNIPAM and Ag-PNIPAM hydrogel.

**Fig. S4.** Bacteriostatic effect of hydrogels.

**Fig. S5.** Bending behavior of Ag nanoparticles hydrogels.

**Fig. S6.** Hydrogels of octopus-like tentacle surfaces.

**Fig. S7.** Bending behavior of hydrogels with different Ag content.

**Fig. S8.** SEM of hydrogels with different Ag content.

**Fig. S9.** Bending angle of hydrogels with different thicknesses.

**Fig. S10.** Bending behavior of hydrogels with different thicknesses.

**Fig. S11.** Comparison of Gauge factor and strain of hydrogels.

**Fig. S12.** Ag nanoparticles hydrogel resistance during heating process.

**Fig. S13.** Hydrogel resistance during dehydration process.

**Fig. S14.** Mechanical response of hydrogels under thermal stimulation.

**Fig. S15.** Hydrogel resistance during heating process at different temperatures.

**Fig. S16.** Conversion of different hydrogel actuators angle definition.

**Movie S1.** Hydrophilicity of two sides of Ag-PNIPAM hydrogel.

**Movie S2.** Bending behavior of Ag-PNIPAM hydrogel.

**Movie S3.** LED circuitry.

**Movie S4.** Four-armed hydrogel gripper.

**Movie S5.** Neuromuscular electrical stimulation electrode on the arm.

**Movie S6.** Circuit switch utilizing thermal response conductivity.

**Movie S7.** Circuit switch combining the unique actuation and conductivity properties.

## Supplementary Notes, Tables and Figures

### Supplementary Note 1. Wettability-based strategy.

It is well known that NIPAM molecules, which contain hydrophilic amide groups and hydrophobic isopropyl groups, exhibit hydrophilic properties during low temperature polymerization. We utilized the introduction of hydrophobic Ag flakes to form the gradient pore structure during the polymerization of PNIPAM hydrogels. The self-gravity of the hydrophobic Ag flakes led to its rapid precipitation at the bottom of the precursor solution, which made it easier for the hydrophilic NIPAM molecules to aggregate at the top side of the hydrogel. It is worth noting that, although the hydrophobicity of the silver flakes leads to the difference in hydrophilicity within the precursor solution, no significant difference in hydrophilicity is reflected on the top and bottom surfaces of the resultant hydrogels. As shown in Movie S1 and Fig. S1, the top and bottom surfaces of the hydrogels with different Ag contents (0.2, 0.3 and 0.4 g) all showed the same superhydrophilicity. This can be explained in two ways:

(1) Although Ag flakes were deposited to the bottom of hydrogel, the silver flakes were only within the hydrogel, not exposed to the surface of the hydrogel.

(2) The Ag contents discussed in this paper are low concentrations relative to the NIPAM content, so it is not sufficient to completely break the strong hydrogen bonds between NIPAM molecules and water molecules, resulting in a substantial shift in hydrophilicity on the hydrogel surface.

**Supplementary Note 2. Octopus-tentacle inspired hydrogel.**

Nature has always been our inspiration source of new materials development. Bioinspired materials are synthetic materials whose structure, properties or functions resemble those of natural materials or living matter. In this paper, we were inspired by octopus-tentacle for the development of Ag-PNIPAM gradient hydrogel.

As we know, the octopus is a soft animal with eight tentacles. The tentacles can have a unique Janus structure, change between transparent and non-transparent, and even be flexibly bent. In this paper, the following three aspects of our gradient hydrogel came from the inspiration of octopus-tentacle:

(1) The hydrogel exhibits Janus surface structure, similar to the shape of octopus-tentacle. (Shape or structure inspiration)

(2) The hydrogel can change between transparent and non-transparent by volume phase transition under temperature stimulation. (Property inspiration)

(3) The hydrogel can undergo ultrafast and flexible bending behaviors through the absorption and release of water under temperature stimulation. (Function inspiration)

Therefore, inspired by octopus-tentacle, our gradient hydrogel resembles octopus-tentacle from Janus surface structure, transparent/non-transparent property and bending function, which is a representative bioinspired material.

**Table S1.** Summarization for the bending speed and bending amplitude of hydrogel actuators.

| Material | Structure | Bending speed | Bending amplitude | Stimulation conditions | Sample size ($mm^3$) | Ref |
|---|---|---|---|---|---|---|
| PNIPAM/ XLG/ HEA | Gradient | 9.8°/s | 206° | 50 °C water | 25 × 5 × 1 | [1] |
| PNIPAM /XLG | Gradient | 2.38°/s | 57.2° | 50 °C water | 25 × 5 × 1 | [2] |
| PNIPAM/ GO | Gradient | 7.5°/s | 360° | NIR 808 nm 2 W $cm^{-2}$ | 20 × 2 × 1 | [3] |
| PNIPAM/ TCNC | Gradient | 9.6°/s | 360° | 40 °C water | —— | [4] |
| PNIPAM /MMT | Gradient | 28.8°/s | 259° | 50 °C water | 50 × 10 × 1 | [5] |
| PNIPAM/ GO | Bilayer | 27.7°/s | 443.4° | 55 °C water | 30 × 10 × 1 | [6] |
| PNIPAM/ XLG/NFC | Bilayer | 9°/s | 180° | 50 °C water | 65 × 7 × 2 | [7] |
| PNIPAM/ XLG/ $MoO_2$ | Bilayer | 3°/s | 90° | NIR 808 nm 0.8 W $cm^{-2}$ | —— | [8] |
| PNIPAM/ P(AAc-co-AAm) | Bilayer | 6.36°/s | 350° | 40 °C oil | 20 × 5 × 2 | [9] |
| PNIPAM/ PAAM-PTCA | Bilayer | 6.1°/s | 305° | 45 °C water | —— | [10] |
| PNIPAM/ Ag | Gradient | 52.3°/s | 559° | 50 °C water | 40 × 10 × 1 | **This work** |

Notes: The data in the tables are converted by the formula (Fig. S16). However, the comparison is only rough because these hydrogels have different sample sizes and stimulation conditions.

**Table S2.** Comparison of the main conductive parameters of Ag-PNIPAM hydrogel and conductive hydrogel strain sensors in previous mainstream work.

| Material | Strain (%) | Gauge Factor | Linear or Nonlinear | Conductive mechanism | Ref |
|---|---|---|---|---|---|
| PAA/NCT | 500 | 2.69 | Linear | Ionic conduction | [11] |
| TA@HAP NWs/PVA(W/EG) | 350 | 2.84 | Linear | Ionic conduction | [12] |
| Ca-GG/PAAm-ZP | 0-120<br>120-250<br>250-500 | 1.76<br>3.6<br>4.68 | Nonlinear | Ionic conduction | [13] |
| PSBMA/CNTs | 0-125<br>125-225<br>225-300 | 2.22<br>5.14<br>10.35 | Nonlinear | Ionic conduction | [14] |
| PVA/GEL/EG /TA@CNC | 0-100<br>100-250<br>250-400 | 1.86<br>2.64<br>4.23 | Nonlinear | Ionic conduction | [15] |
| HF(PVA-C/P) | 400 | 2.1 | Linear | Electronic conduction | [16] |
| MWCNTs-PDMS | 160 | 3.77 | Linear | Electronic conduction | [17] |
| AAm/HEMA/MXene /AgNPs | 0-60<br>60-100<br>100-120 | 3.36<br>3.72<br>4.08 | Nonlinear | Electronic conduction | [18] |
| PVA/G/PDA/AgNPs | 0-70<br>70-315 | 0.94<br>0.13 | Nonlinear | Electronic conduction | [19] |
| MWCNT/PVA/PAAm | 100-300<br>300-500 | 2.32<br>4.02 | Nonlinear | Electronic conduction | [20] |
| PNIPAM/Ag | 500 | 14.66 | Linear | Electronic conduction | **This work** |

**Table S3.** Summarization for the gripping time and the releasing time of hydrogel gripper.

| **Material** | **Structure** | **Gripping time** | **Releasing time** | **Gripping conditions** | **Releasing conditions** | **Ref** |
|---|---|---|---|---|---|---|
| PNIPAM /TCNC | Gradient | 18 s | 104 s | 40 ℃ water | 25 ℃ water | [4] |
| PNIPAM /MMT | Gradient | 9 s | 568 s | 50 ℃ water | 20 ℃ water | [5] |
| PNIPAM/ PDA-EGaIn | Gradient | 18 s | 24 s | 45 ℃ water | 45 ℃ water | [21] |
| NaSS-co-DMAEA-Q | Gradient | 55 min | 10 min | DI water | 2 M NaCl | [22] |
| PNIPAM/ P(AAc-co-AAm) | Bilayer | 5 min | 4 min | 80 ℃ hot plate | Ice-cold plate | [9] |
| PNIPAAm/ PNIPAAm-SP | Bilayer | 30 s | 180 s | 35 ℃ water | 25 ℃ water | [23] |
| PNIPAM/ PDMAEMA | Bilayer | 15 s | 30 s | 45 ℃ water | 15 ℃ water | [24] |
| NMAM | Bilayer | 5 min | 3 min | $Fe^{3+}$ solution | Air | [25] |
| PNIPAM/Ag | Gradient | 8 s | 1 s | 50 ℃ water | 20 ℃ water | **This work** |

Notes: The comparison is only rough because these hydrogels have different sample sizes and stimulation conditions.

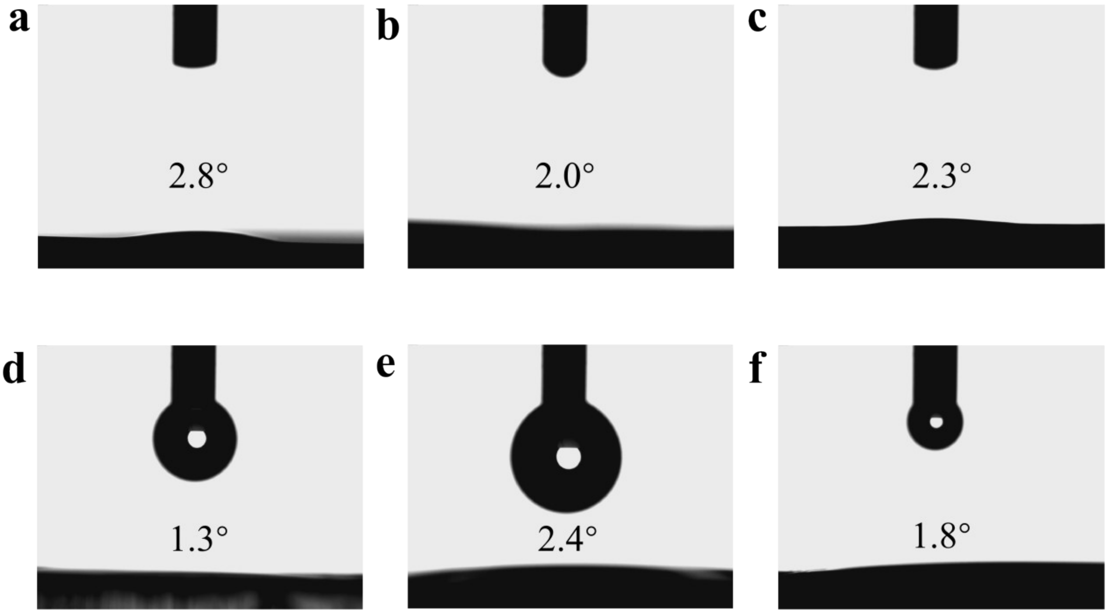


**Fig. S1.** The water contact angles of Ag-PNIPAM hydrogel. The top side of (a) $Ag_{0.2}$-PNIPAM, (b) $Ag_{0.3}$-PNIPAM, (c) $Ag_{0.4}$-PNIPAM. The bottom side of (d) $Ag_{0.2}$-PNIPAM, (e) $Ag_{0.3}$-PNIPAM, (f) $Ag_{0.4}$-PNIPAM.

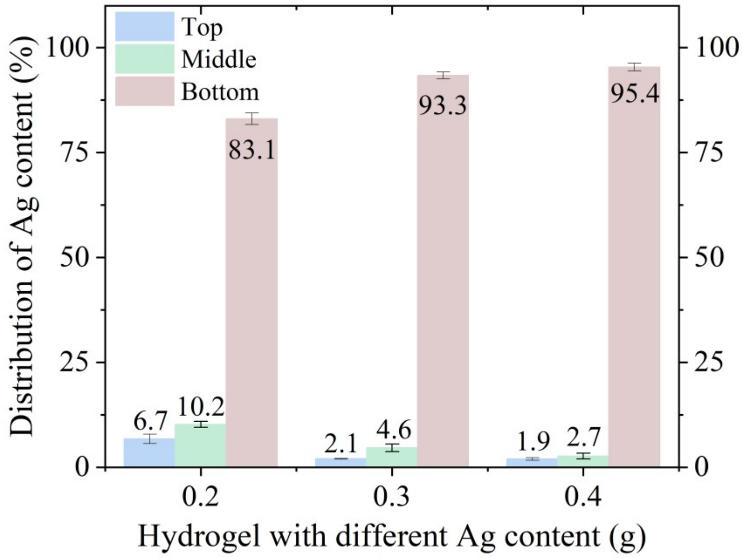


**Fig. S2.** Distribution of Ag content in Ag-PNIPAM hydrogel.

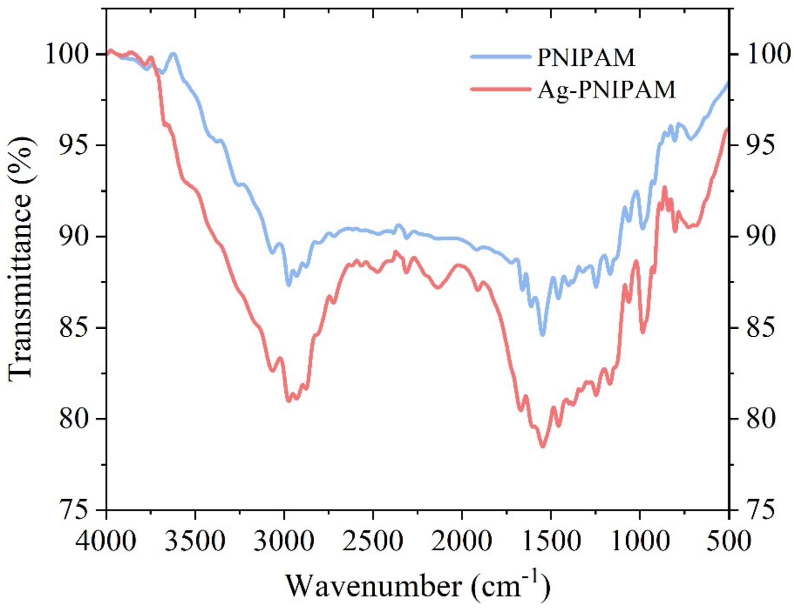


**Fig. S3.** FTIR spectra of pure PNIPAM and Ag-PNIPAM hydrogel.

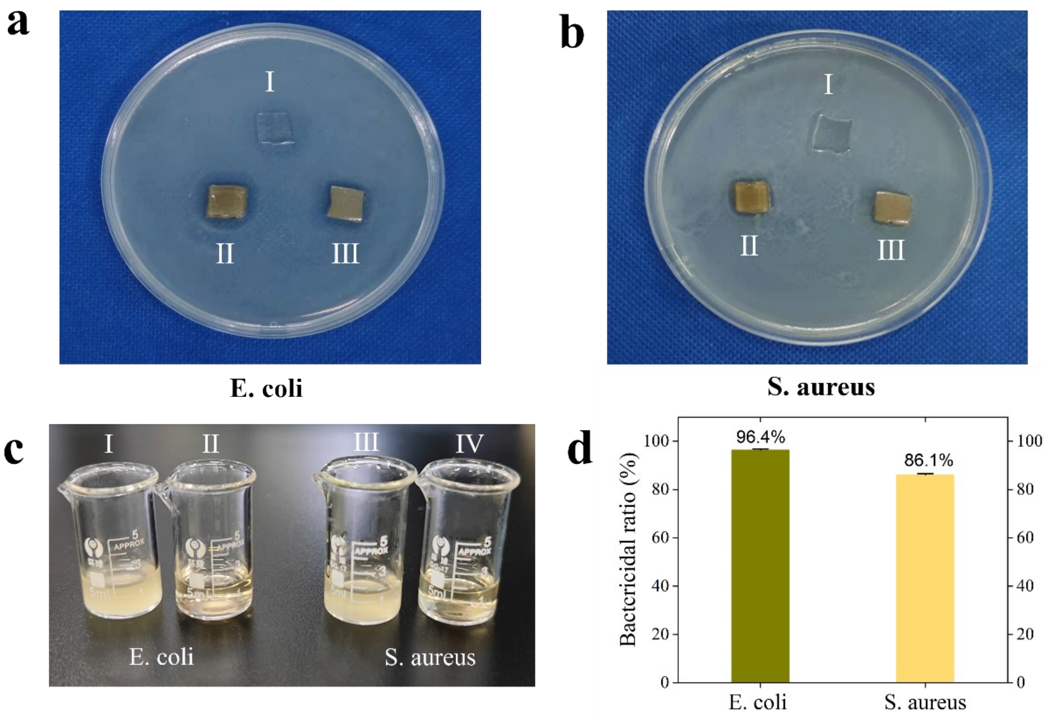


**Fig. S4.** Bacteriostatic effect of hydrogels. Antibacterial performance of Ag-PNINAM hydrogel against (a) E. coli and (b) S. Aureus; I. Pure PNIPAM; II. The bottom side of Ag-PNIPAM; III. The top side of Ag-PNIPAM. (c) Comparison of bacterial suspensions before and after putting in hydrogel. I. Bacterial suspension of E. coli, II. Bacterial suspension of E. coli after adding Ag-PNIPAM hydrogel, III. Bacterial suspension of S. aureus, IV. Bacterial suspension of S. aureus after adding Ag-PNIPAM hydrogel. (d) The bactericidal ratio of the Ag-PNIPAM hydrogels to E. coli and S. aureus.

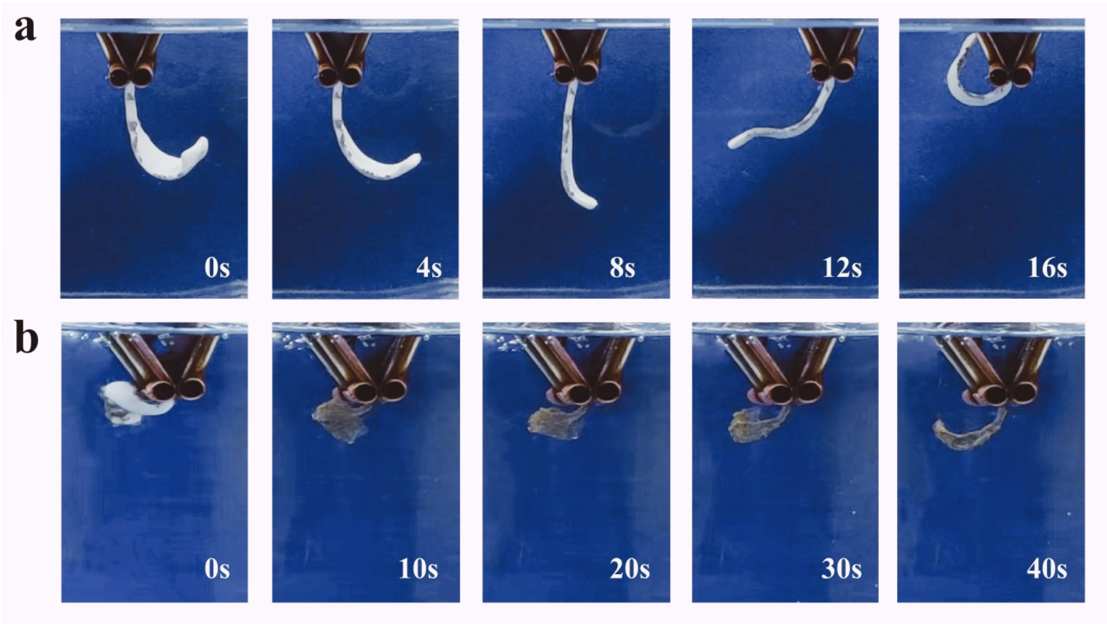


**Fig. S5.** Bending behavior of Ag nanoparticles hydrogels. Ag nanoparticle hydrogel (a) in water at 50 °C, (b) in water at 20 °C.

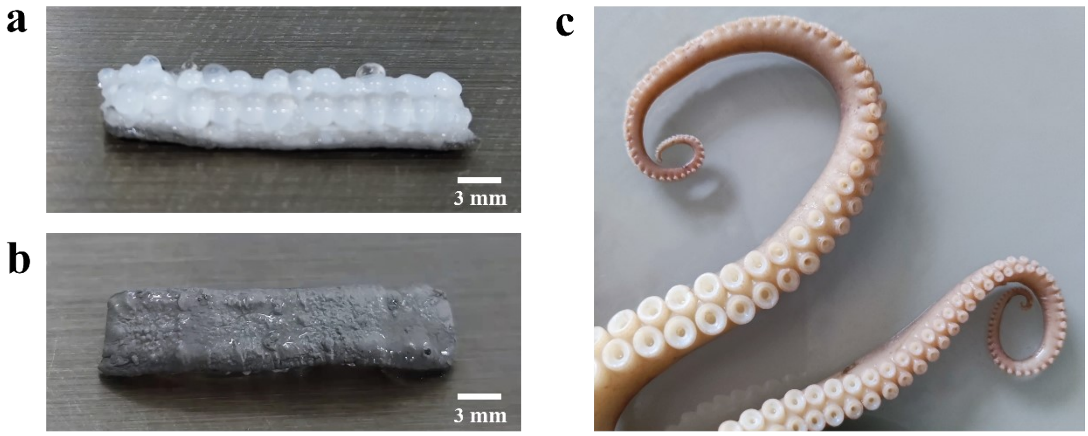


**Fig. S6.** Hydrogels of octopus-like tentacle surfaces. Ag-PNIPAM hydrogel (a) top and (b) bottom surfaces at 50 ℃. (c) Octopus-tentacle.

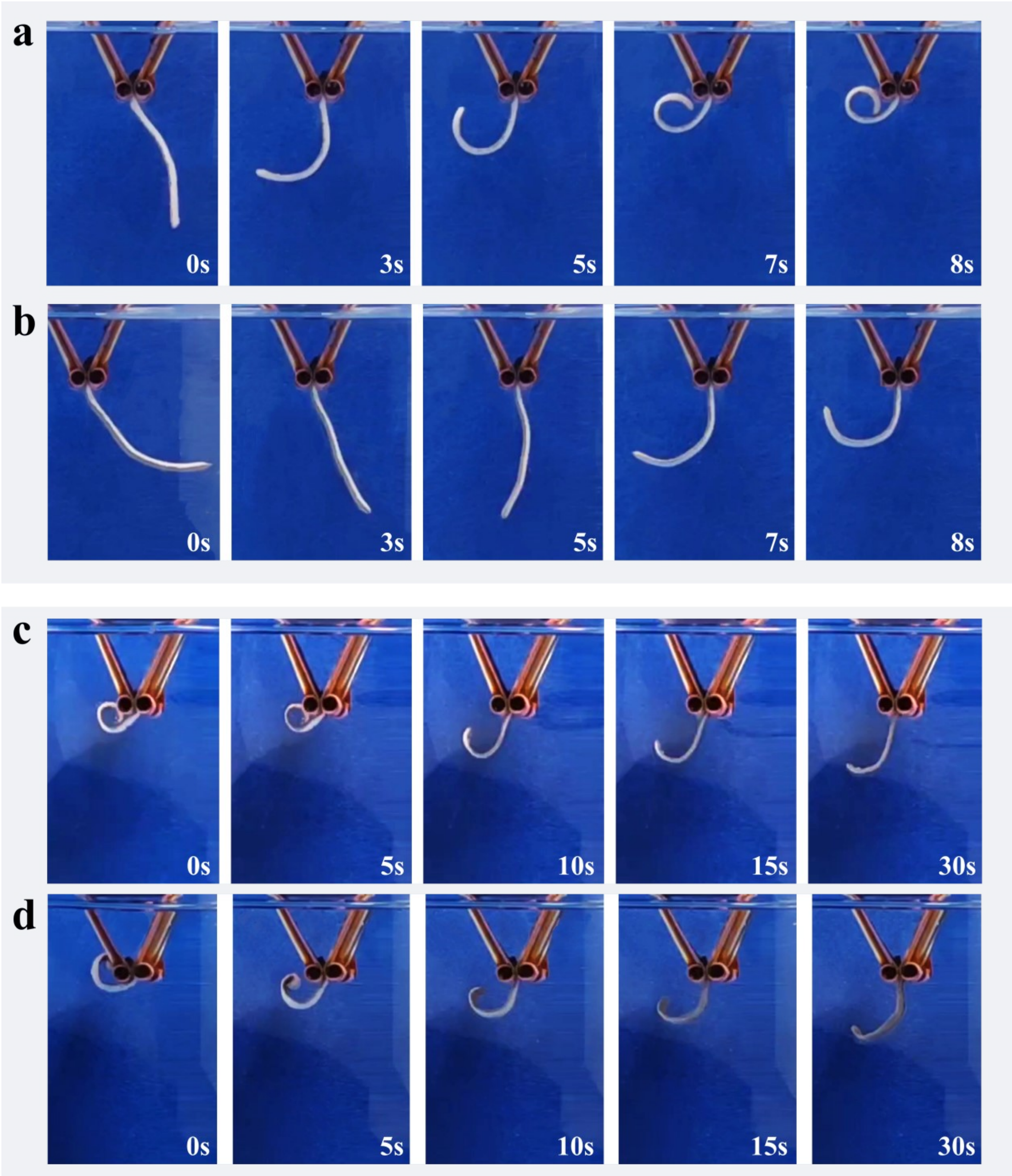


**Fig. S7.** Bending behavior of hydrogels with different Ag content. The bending behavior of (a) $Ag_{0.2}$-PNIPAM and (b) $Ag_{0.4}$-PNIPAM hydrogel with a thickness of 1 mm in water at 50 °C. The bending behavior of (c) $Ag_{0.2}$-PNIPAM and (d) $Ag_{0.4}$-PNIPAM hydrogel with a thickness of 1 mm in water at 20 °C.

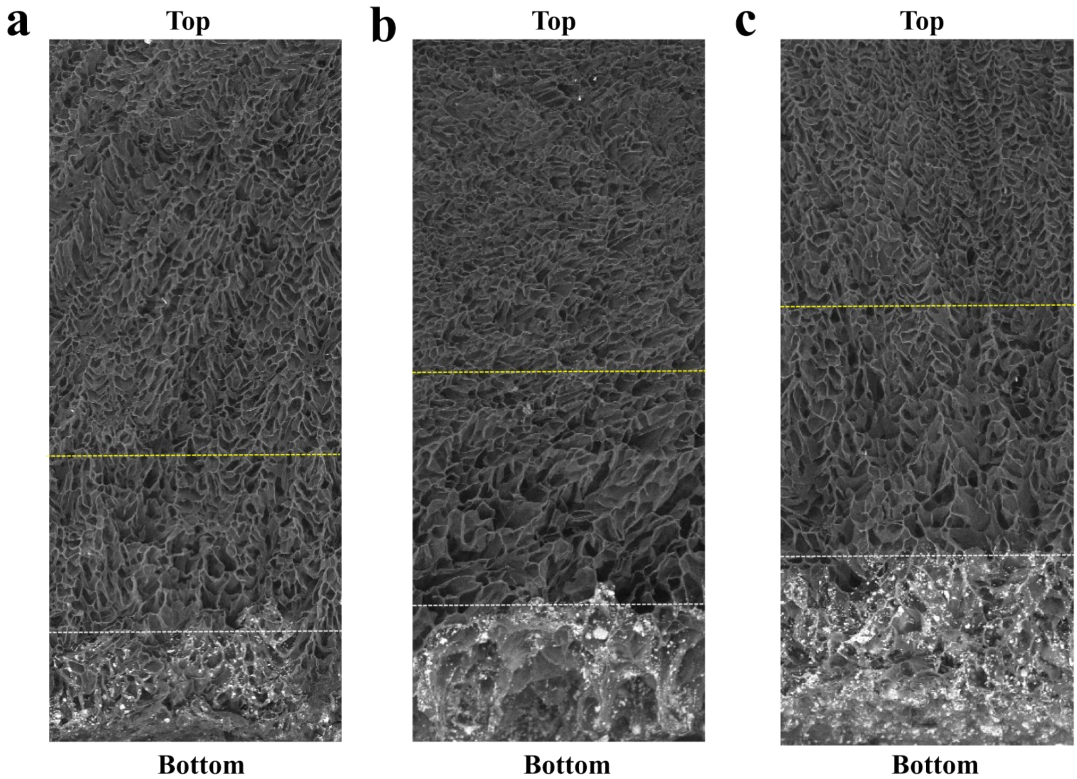


**Fig. S8.** SEM of hydrogels with different Ag content. SEM of freeze-dried (a) $Ag_{0.2}$-PNIPAM, (b) $Ag_{0.3}$-PNIPAM and (c) $Ag_{0.4}$-PNIPAM hydrogel with large-ranged gradient structure along the direction of gravity. Among them, the yellow and white lines roughly delineate the distribution of larger pore sizes and Ag flakes, respectively.

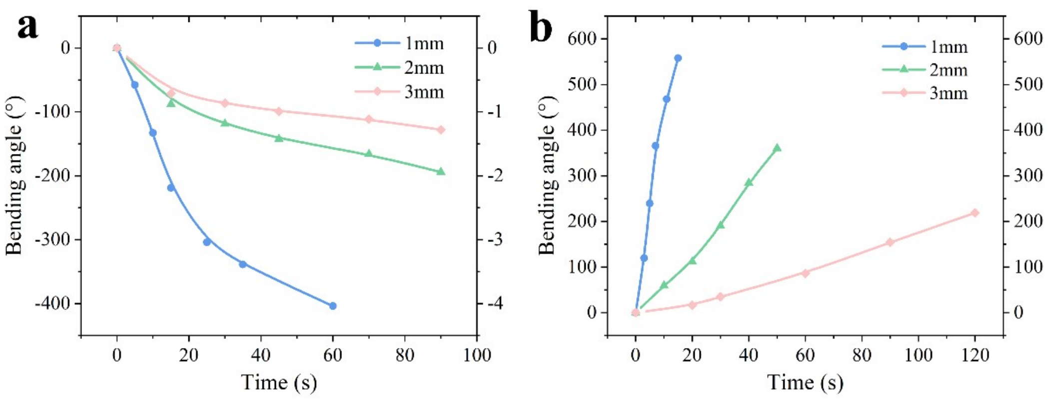


**Fig. S9.** Bending angle of hydrogels with different thicknesses. Effect of thickness of $Ag_{0.3}$-PNIPAM hydrogels on bending response in water at (a) 50 °C and (b) 20 °C.

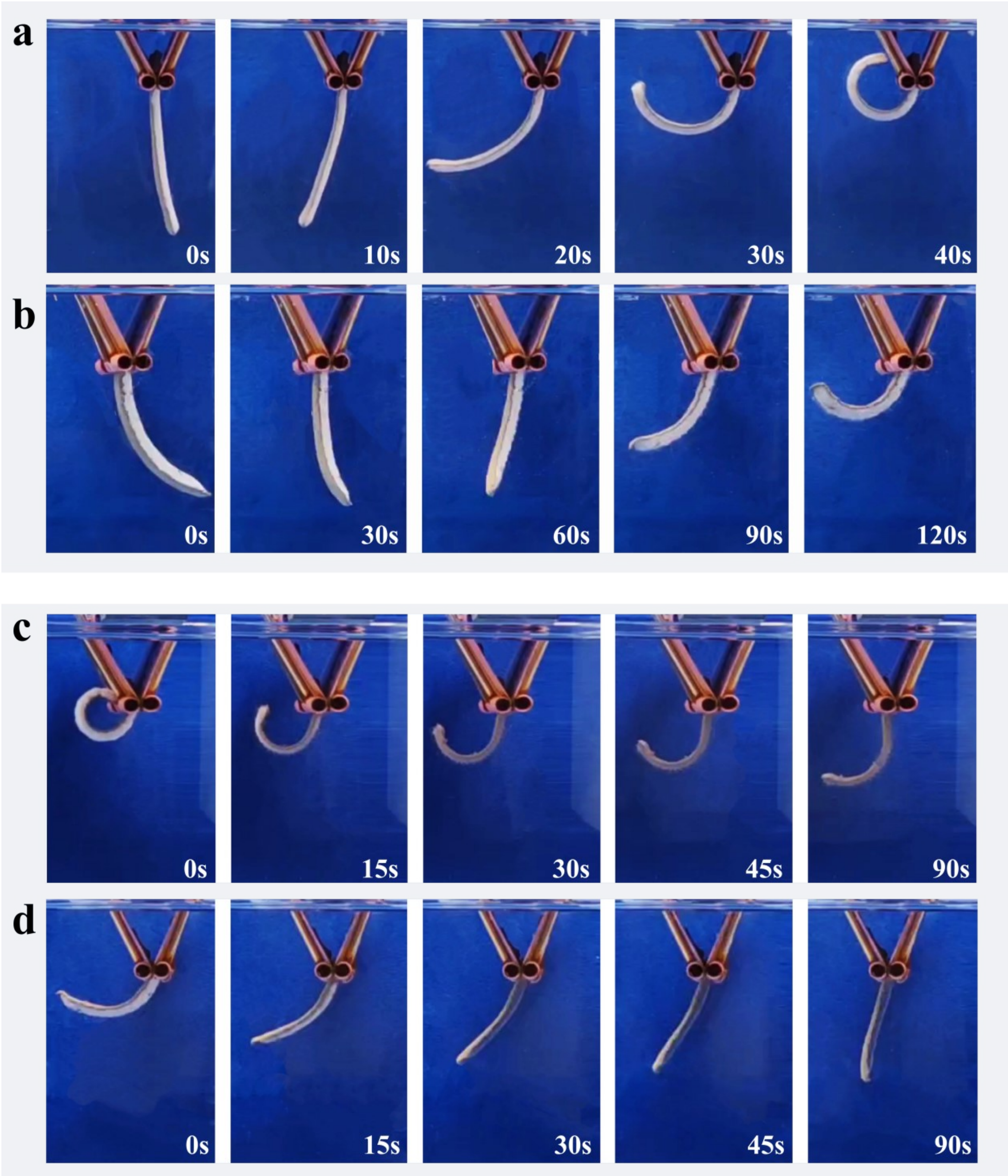


**Fig. S10.** Bending behavior of hydrogels with different thicknesses. The bending behavior of $Ag_{0.3}$-PNIPAM hydrogel with a thickness of (a) 2 mm and (b) 3 mm in water at 50 °C. The bending behavior of $Ag_{0.3}$-PNIPAM hydrogel with a thickness of (c) 2 mm and (d) 3 mm in water at 20 °C.

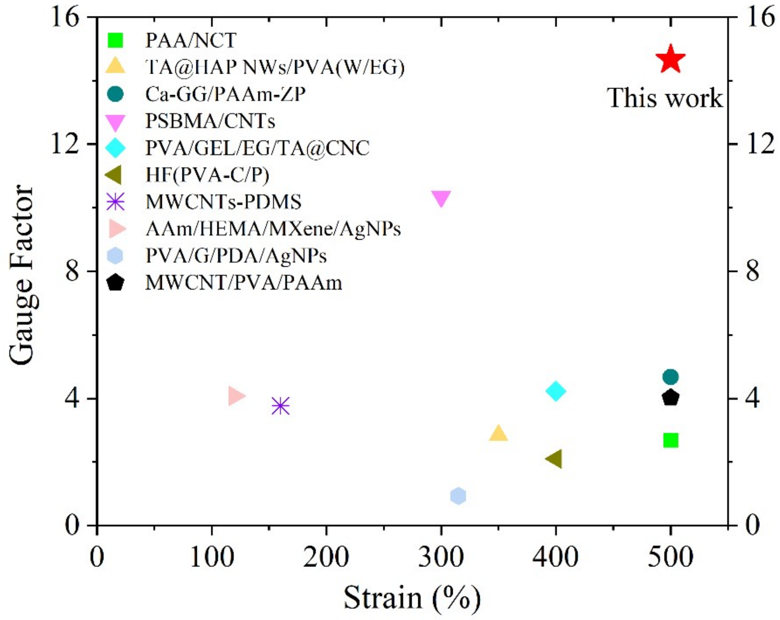


**Fig. S11.** Comparison of Gauge factor and strain of hydrogels. Comparison of gauge factor within the strain of 500% of some typical reported strain sensors (see details in Table S2).

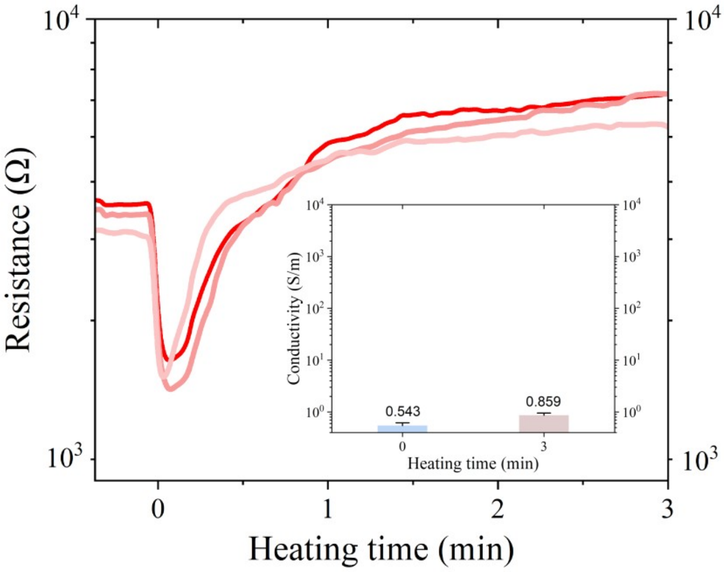


**Fig. S12.** Ag nanoparticles hydrogel resistance during heating process. Resistance changes of Ag nanoparticles hydrogels in water at 50 °C and (inset) conductivity at 0 min and 3 min with 3 samples.

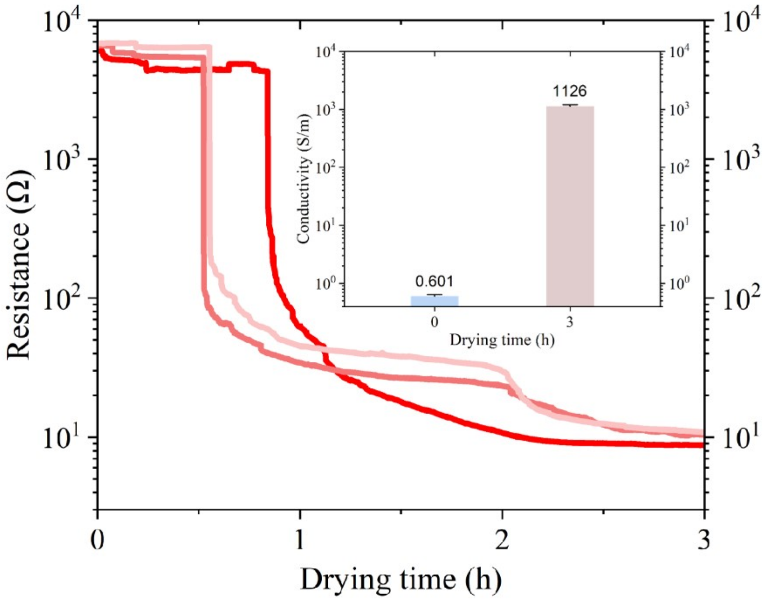


**Fig. S13.** Hydrogel resistance during dehydration process. Resistance changes of $Ag_{0.3}$-PNIPAM hydrogels at room temperature drying conditions and (inset) conductivity at 0 h and 3 h with 3 samples.

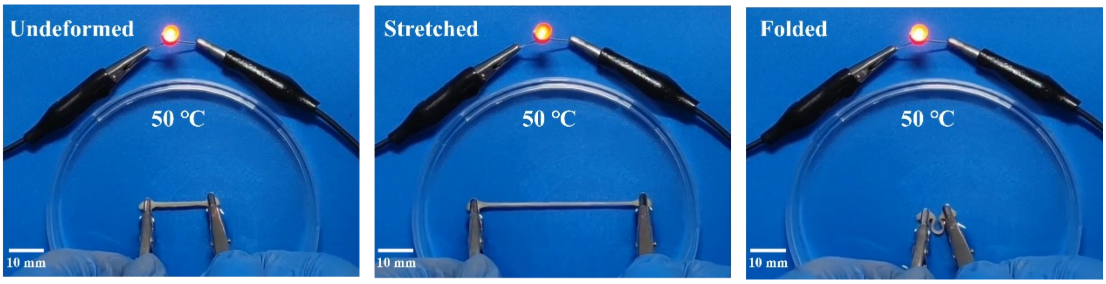


**Fig. S14.** Mechanical response of hydrogels under thermal stimulation. Brightness changes of LED in the undeformed, stretched and folded states of $Ag_{0.3}$-PNIPAM hydrogels in 50 ℃ water.

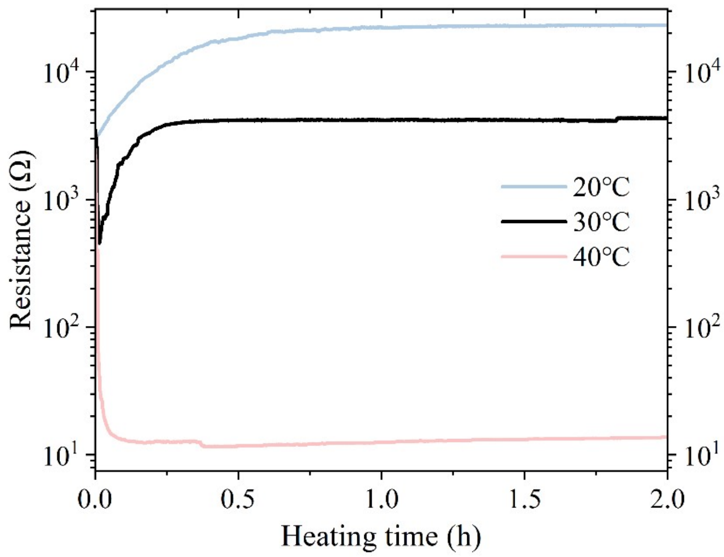


**Fig. S15.** Hydrogel resistance during heating process at different temperatures. Resistance changes of $Ag_{0.3}$-PNIPAM hydrogels in water at 20 °C, 30 °C and 40 °C, respectively.

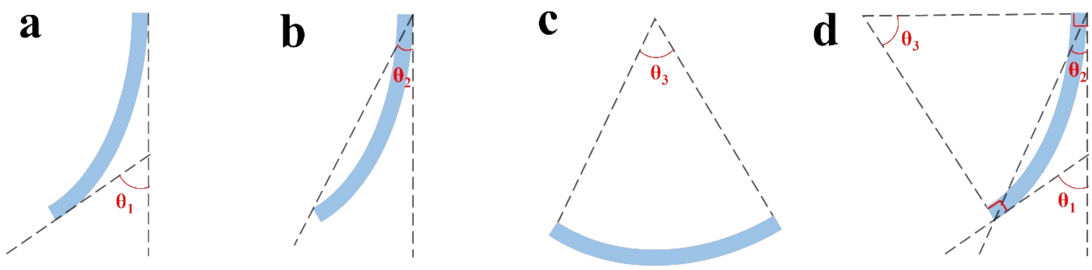


**Fig. S16.** Conversion of different hydrogel actuators angle definition. Since bending angles are defined differently in different researches, the following three main ways of defining bending angles are listed (a-c) and unified (d) in order to facilitate comparison with other researches. It is easy to know: $\theta_1 = 2\theta_2 = \theta_3$.

## Reference


1. Y. Tan, D. Wang, H. Xu, Y. Yang, X. L. Wang, F. Tian, P. Xu, W. An, X. Zhao and S. Xu, *ACS Appl. Mater. Interfaces*, 2018, **10**, 40125-40131.
2. Y. Tan, D. Wang, H. Xu, Y. Yang, W. An, L. Yu, Z. Xiao and S. Xu, Macromol Rapid Commun, 2018, **39**, e1700863.
3. Y. Yang, Y. Tan, X. Wang, W. An, S. Xu, W. Liao and Y. Wang, ACS Appl. Mater. Interfaces, 2018, **10**, 7688-7692.
4. K. Mo, M. He, X. Cao and C. Chang, J. Mater. Chem. C, 2020, **8**, 2756-2763.
5. J. Liu, W. Xu, Z. Kuang, P. Dong, Y. Yao, H. Wu, A. Liu and F. Ye, J. Mater. Chem. C, 2020, **8**, 12092-12099.
6. X. M. He, Y. Sun, J. H. Wu, Y. Wang, F. Chen, P. Fan, M. Q. Zhong, S. W. Xiao, D. Zhang, J. T. Yang and J. Zheng, J. Mater. Chem. C, 2019, **7**, 4970-4980.
7. Q. Zhao, Y. Liang, L. Ren, Z. Yu, Z. Zhang, F. Qiu and L. Ren, J Mater Chem B, 2018, **6**, 1260-1271.
8. Z. Sun, C. Wei, W. Liu, H. Liu, J. Liu, R. Hao, M. Huang and S. He, ACS Appl. Mater. Interfaces, 2021, **13**, 33404-33416.
9. J. Zheng, P. Xiao, X. Le, W. Lu, P. Théato, C. Ma, B. Du, J. Zhang, Y. Huang and T. Chen, J. Mater. Chem. C, 2018, **6**, 1320-1327.
10. B. Y. Wu, X. X. Le, Y. K. Jian, W. Lu, Z. Y. Yang, Z. K. Zheng, P. Theato, J. W. Zhang, A. Zhang and T. Chen, Macromol Rapid Commun, 2019, **40**, e1800648.
11. X. Jing, P. Feng, Z. Chen, Z. Xie, H. Li, X.-F. Peng, H.-Y. Mi and Y. Liu, ACS Sustainable Chem. Eng., 2021, **9**, 9209-9220.
12. J. Wen, J. Tang, H. Ning, N. Hu, Y. Zhu, Y. Gong, C. Xu, Q. Zhao, X. Jiang, X. Hu, L. Lei, D. Wu and T. Huang, Adv. Funct. Mater., 2021, **31**, 2011176.
13. Q. Jiao, L. Cao, Z. Zhao, H. Zhang, J. Li and Y. Wei, Biomacromolecules, 2021, **22**, 1220-1230.
14. X. Sun, S. He, Z. Qin, J. Li and F. Yao, Compos. Commun., 2021, **26**, 100784.
15. J. Yin, C. Lu, C. Li, Z. Yu, C. Shen, Y. Yang, X. Jiang and Y. Zhang, Composites, Part B, 2022, **230**, 109528.
16. Q. Zhang, Q. Wang, G. Wang, Z. Zhang, S. Xia and G. Gao, ACS Appl. Mater. Interfaces, 2021, **13**, 50411-50421.
17. K. Zhang, C. Song, Z. Wang, C. Gao, Y. Wu and Y. Liu, J. Mater. Chem. C, 2020, **8**, 17277-17288.
18. Z. Wang, X. Zhang, T. Cao, T. Wang, L. Sun, K. Wang and X. Fan, ACS Appl. Mater. Interfaces, 2021, **13**, 46022-46032.
19. L. Fan, J. Xie, Y. Zheng, D. Wei, D. Yao, J. Zhang and T. Zhang, ACS Appl. Mater. Interfaces, 2020, **12**, 22225-22236.
20. B. Cheng, Y. Li, H. Li, H. Li, S. Yang, P. Li and Y. Shang, Compos. Sci. Technol., 2021, **213**, 108948.
21. Y. Chen, Z. Chen, C. Chen, H. Ur Rehman, H. Liu, H. Li and M. S. Hedenqvist, Chem. Eng. J., 2021, **421**, 127762.
22. Z. Shao, S. Wu, Q. Zhang, H. Xie, T. Xiang and S. Zhou, Polym. Chem., 2021, **12**, 670-679.
23. X. Zhang, X. Xu, L. Chen, C. Zhang and L. Liao, Dyes Pigm., 2020, **174**, 108042.
24. Y. Cheng, K. Ren, D. Yang and J. Wei, Sens. Actuators, B, 2018, **255**, 3117-3126.
25. H. Ding, X. Liang, S. Y. Zheng, Q. Wang, Z. Li and G. Sun, Mater. Chem. Phys., 2020, **253**, 123332.